Unmanned Systems, Vol. 8, No. 3 (2020) 239–251
© World Scientific Publishing Company
DOI: 10.1142/S230138502050017X

UNMANNED SYSTEMS
https://www.worldscientific.com/worldscinet/us

Un. Sys. 2020.08:239-251. Downloaded from www.worldscientific.com
by CHINESE UNIVERSITY OF HONG KONG on 08/08/20. Re-use and distribution is strictly not permitted, except for Open Access articles.

# Mechanical Impedance Control of Cooperative Robot During Object Manipulation Based on External Force Estimation Using Recurrent Neural Network

Misaki Hanafusa*, Jun Ishikawa

*Department of Robotics and Mechatronics, Tokyo Denki University,*
*5 Senju Asahi-cho, Adachi-ku,*
*Tokyo, 120-8551, Japan*

This paper proposes a compliant motion control for human-cooperative robots to absorb collision force when persons accidentally touch the robots even while the robot is manipulating an object. In the proposed method, an external force estimator, which can distinguish the net external force from the object manipulation force, is realized using an inverse dynamics model acquired by a recurrent neural network (RNN). By implementing a mechanical impedance control to the estimated external force, the robot can quickly and precisely carry the object keeping the mechanical impedance control functioned and can generate a compliant motion to the net external force only when the person touches it during manipulation. Since the proposed method estimates the external force from the generalized force based on the learned inverse dynamics, it is not necessary to install any sensors on the manipulated object to measure the external force. This allows the robot to detect the collision even when the person touches anywhere on the manipulated object. The RNN inverse dynamics model is evaluated by the leave-one-out cross-validation and it was found that it works well for unknown trajectories excluded from the learning process. Although the details were omitted due to the limitation of the page length, similar to the simulations, the RNN inverse dynamics model was evaluated using unknown trajectories in the six degree-of-freedom experiments, and it has been verified that it functions properly even for the unknown trajectories. Finally, the validity of the proposed method has been confirmed by experiments in which a person touches a robot while it is manipulating an object with six degrees of freedom.

*Keywords*: Soft robotics; recurrent neural network; external force estimation; human-cooperative robot.

US

## 1. Introduction

Industry 4.0 proposed by Germany aims to realize sophisticated production system, and Society 5.0 in Japan proposes a concept of the smart factory. In the prospects, it is expected to realize flexible production lines by reconfigurable robots that can perform small lot production of many kinds of products [1]. Some of these robots are supposed to collaborate with humans, and in Japan, it is said that more powerful robots will be used as boosted by deregulation for the 80 W limitation to the actuators [2]. These collaborative robots are desired to flexibly and safely work with humans with the quick and precise motion keeping. For example, in industry, various safeguarding technologies from both hard and soft safety considerations are implemented for high-payload robots [3].

As examples of the collision detections, a method using joint torque sensors [4], a sensorless method [5], and a disturbance observer (DOB) application to reduce false detection [6] have been proposed. Various mechanisms to reduce the collision impact have also been proposed such as application of nonlinear stiffness [7], an approach aiming for both high stiffness and light weight [8], a comparative evaluation of tendon and direct driving [9], a passive joint to absorb the impact [10], and an magnetorheological fluid clutch [11]. Also, in order to flexibly collaborate with humans, it is known as an effective method to increase the back drivability, and many methods for improving it have been proposed (see [12, 13]). As a solution

Received 2 December 2019; Revised 1 February 2020; Accepted 1 February 2020; Published 20 July 2020. This paper was recommended for publication in its revised form by editorial board member, Han Wang.
Email Address: *hanafusa@robotics.fr.dendai.ac.jp.

Un. Sys. 2020.08:239-251. Downloaded from www.worldscientific.com
by CHINESE UNIVERSITY OF HONG KONG on 08/08/20. Re-use and distribution is strictly not permitted, except for Open Access articles.

for the issue, it has recently been reported to utilize series elastic actuators (SEAs) in the field of welfare [14–16], exoskeletons [17], and cooperative robots [18].

One of the key technologies common to the above studies is to precisely measure the external force applied by the environment in simple and inexpensive ways. Thus, it is a challenge to estimate the external force/torque, distinguishing it from the generalized force needed for both the robot actuation and the object manipulation while the robot is carrying the object. For example, in [19], a method to estimate the net external force/torque using a DOB [20] has been proposed. In order to apply the linear DOB to nonlinear systems such as robots, however, complicated control is generally needed to linearize the dynamics by using nonlinear feedback based on the parameter values of the robot [8]. As a solution to the problem, recurrent neural networks (RNNs) have been utilized by which the inverse dynamics are acquired to express the nonlinear input–output relationship [21–25]. In this paper, an external force estimator is proposed using a RNN that acquires an inverse dynamics model of a robot manipulating an object. In the proposed method, the net external force/torque is estimated from the difference between the actually measured force/torque generated by the joints and the force/torque required for robot motion. Then a mechanical impedance control is proposed in which the compliant motion to the net external force/torque in collision with the environment is generated even when the robot is dynamically and accurately manipulating the object. The validity of the proposed method is confirmed by experiments of six degree of freedom (DOF) object manipulation by a robot (PA10-7C).

## 2. External Force Estimator Using RNN

### 2.1. *Inverse dynamics model acquisition by learning*

Let $\boldsymbol{\theta}$ be the generalized coordinate, $\boldsymbol{\tau}$ the generalized force, an equation of motion of a robot is generally given by

$$\boldsymbol{\tau} + \mathbf{J}^{\mathrm{T}} \cdot \mathbf{f}_d = \mathbf{M} \cdot \ddot{\boldsymbol{\theta}} + \mathbf{h} + \mathbf{D} \cdot \dot{\boldsymbol{\theta}} + \mathbf{g}, \tag{1}$$

where $\mathbf{M}$ is an inertia matrix, $\mathbf{h}$ is a term of centrifugal force and Coriolis force, $\mathbf{D} \cdot \dot{\boldsymbol{\theta}}$ is a term of viscous friction, and $\mathbf{g}$ is a gravity term. Also, $\mathbf{f}_d$ is the external force in the absolute coordinate space, and $\mathbf{J}$ is the Jacobian matrix. In this section, a method to acquire an inverse dynamics model to calculate the generalized force from the robot motion by using a RNN is quickly reviewed [25].

In the proposed method, an RNN is used to estimate the generalized force $\boldsymbol{\tau}$ from the generalized coordinate $\boldsymbol{\theta}$. Figure 1 shows the configuration of the proposed RNN inverse dynamics model with $N$ tap delays. In addition to the estimate $\tilde{\boldsymbol{\theta}}$ of the generalized coordinate, the estimates of the differentials, $\dot{\tilde{\boldsymbol{\theta}}}$ and $\ddot{\tilde{\boldsymbol{\theta}}}$, are also used as the input vector. More specifically, by using an observer having the same configuration as a general type1 DOB, its input is set to zero so that the state corresponding to the disturbance can be used as the angular acceleration estimate (hereinafter referred to as DOB-type differentiator).

The input vector $\mathbf{x}_N \in \Re^{N_I \times 1}$ of the RNN is the states of the DOB-type differentiator $\mathbf{x}_N = [\,\tilde{\theta}^{\mathrm{T}} \quad \dot{\tilde{\theta}}^{\mathrm{T}} \quad \ddot{\tilde{\theta}}^{\mathrm{T}}\,]^{\mathrm{T}}$, and the output vector $\mathbf{y}_N \in \Re^{N_O \times 1}$ is the generalized force $\boldsymbol{\tau}_N$. Then, let the output vector of the hidden layer be $\mathbf{h}_N \in \Re^{N_H \times 1}$, the output of the RNN is calculated as

$$\begin{aligned}\mathbf{h}_N[k] = \sigma_t(&\mathbf{b}_n + \mathbf{W}_x \cdot \mathbf{x}_N[k] \\ &+ \mathbf{W}_h \cdot [\mathbf{h}_N[k-1]^{\mathrm{T}}, \\ &\mathbf{h}_N[k-2]^{\mathrm{T}}, \ldots, \mathbf{h}_N[k-N]^{\mathrm{T}}]^{\mathrm{T}}),\end{aligned} \tag{2}$$

$$\mathbf{y}_N[k] = \mathbf{b}_o + \mathbf{W}_o \cdot \mathbf{h}_N[k]. \tag{3}$$

The activation function $\sigma_t(u)$ of the hidden layer is a hyperbolic tangent sigmoid function, and the output layer activation function is a linear function.

### 2.2. *External force estimation based on RNN inverse dynamics model*

The proposed external force estimator calculates the net external force from the difference between the force/torque

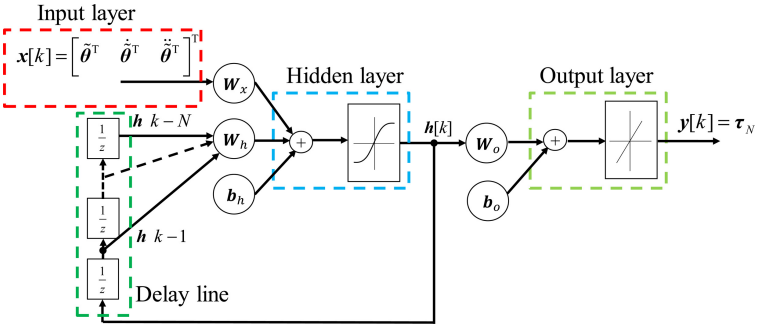


Fig. 1. Proposed inverse dynamics model using RNN: RNN estimates generalized force from robot motion.

Un. Sys. 2020.08:239-251. Downloaded from www.worldscientific.com
by CHINESE UNIVERSITY OF HONG KONG on 08/08/20. Re-use and distribution is strictly not permitted, except for Open Access articles.

$\boldsymbol{\tau}$ generated by the robot and the force/torque $\boldsymbol{\tau}_N$ nominally needed for the robot motion and object manipulation (Fig. 2). Here, $\boldsymbol{\tau}$ is the generalized force including the influence of the external force, and $\boldsymbol{\tau}_N$ is the nominal force/torque generated by the RNN inverse dynamics model trained in the case that the no external force is applied. Note that the force/torque generated by the joint can be measured from the current when the motors are highly backdrivable or from the spring displacement in using SEA. For learning, a method of back-propagation based on Bayesian Regularization [26] is used. Thus, the estimate of the external force/torque in the joint coordinate space can be calculated from the measured joint force/torque and the RNN output as follows:

$$\hat{\boldsymbol{\tau}}_d = \boldsymbol{\tau}_N - \boldsymbol{\tau}. \tag{4}$$

Note that the definition of the direction of $\boldsymbol{\tau}$ and $\boldsymbol{\tau}_d$ is opposite. Finally, the estimate of the external force $\hat{\boldsymbol{f}}_d$ in the absolute coordinate space is obtained by

$$\hat{\boldsymbol{f}}_d = (\mathbf{J}^{\mathrm{T}})^{-1}\hat{\boldsymbol{\tau}}_d. \tag{5}$$

The advantages of the RNN inverse dynamics model are summarized as follows:

— The values of physical parameters of the robot are not needed to obtain inverse dynamics model.
— If the friction force and parameter perturbation, which are difficult to be modeled, have reproducibility, an inverse dynamics model can be acquired.

The effectiveness of the proposed external force estimator will be verified in detail from Sec. 3 by experiments.

## 3. Mechanical Impedance Control Based on RNN External Force Estimation

### 3.1. *Estimation of external force applied to object manipulated by robot*

This section discusses to apply the proposed external force estimator to estimate the external force applied to the object manipulated by a robot. First, considering the case that the generalized force needed for the object manipulation can be directly measured, the relationship between the motion of the manipulated object and the manipulation force generated by the robot with no external force added, i.e. an inverse dynamics, is learned by an RNN. Then, by using the RNN inverse dynamics model, the collision force when a person contacts the object becomes to be able to be detected as an external force even while the robot is manipulating the object.

Figure 3 shows the absolute coordinate system $R$ and the object coordinate system $B$ fixed to the object operated by the robot. The origin of the coordinate system $B$ is fixed to the center of mass (COM) of the object, and the position $[x \quad y \quad z]^{\mathrm{T}}$ observed from the absolute coordinate system $R$ is defined to be zero at the position that the motion is to be started, without loss of generality. Here, what is learned as an RNN inverse dynamics model is the equation of motions of the object moving in the three-dimensional space given by

$$\begin{aligned} {}^{B}\mathbf{f} &= m \cdot {}^{B}\ddot{\mathbf{s}}, \\ {}^{B}\boldsymbol{\tau} &= {}^{B}\mathbf{I} \cdot {}^{B}\dot{\boldsymbol{\omega}} + {}^{B}\boldsymbol{\omega} \times ({}^{B}\mathbf{I} \cdot {}^{B}\boldsymbol{\omega}), \end{aligned} \tag{6}$$

where the superscript $B$ indicates that the variables are observed from the coordinate system $B$ (this superscript is omitted when the variables are observed in the reference

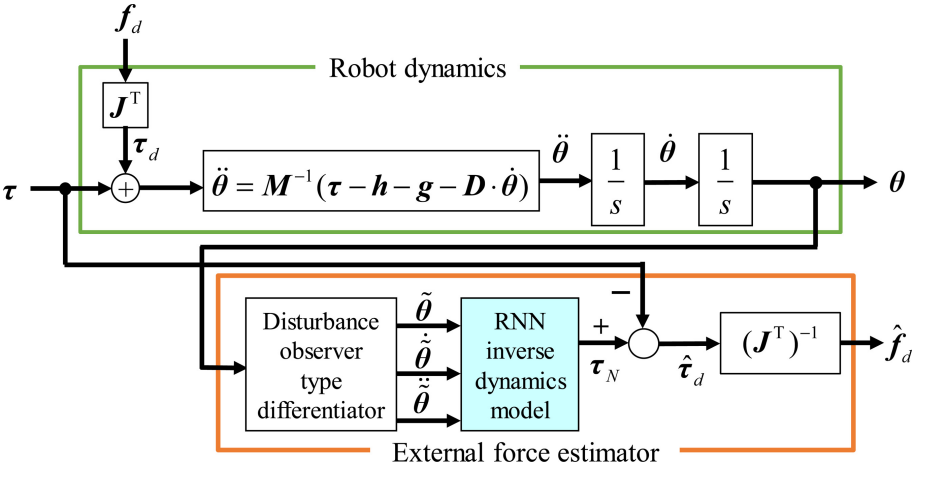


Fig. 2. Proposed external force estimator using RNN inverse dynamics model: the estimate $\hat{\boldsymbol{\tau}}_d$ is calculated as the difference between $\boldsymbol{\tau}$ and $\boldsymbol{\tau}_N$. The estimate $\hat{\boldsymbol{\tau}}_d$ can be projected to $\hat{\mathbf{f}}_d$ in the absolute coordinate space.

Un. Sys. 2020.08:239-251. Downloaded from www.worldscientific.com
by CHINESE UNIVERSITY OF HONG KONG on 08/08/20. Re-use and distribution is strictly not permitted, except for Open Access articles.

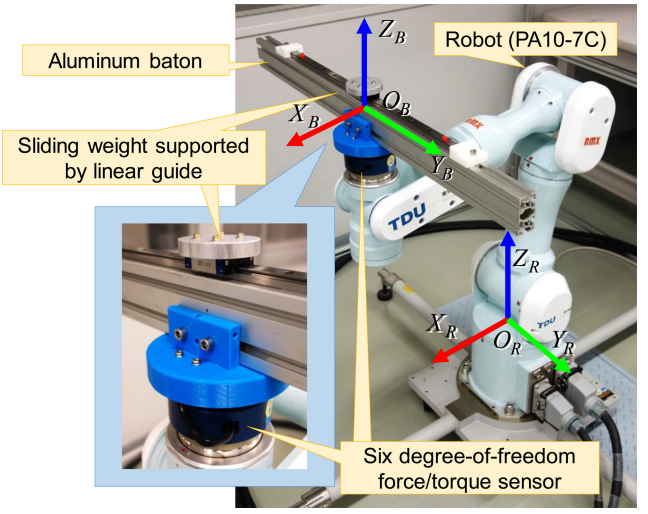


Fig. 3. Definitions of the absolute coordinate system $R$ and the object coordinate system $B$: The coordinate systems are displayed on the experimental robot system, in which the robot can manipulate an aluminum baton. The detail of the experimental setup is given in Sec. 4.1.

coordinate system $R$). In addition, $m$ and ${}^B\mathbf{I}$ are the mass and inertia tensor of the object, ${}^B\ddot{\boldsymbol{s}}$ is the acceleration of the COM, ${}^B\boldsymbol{\omega}$ is the angular velocity, and ${}^B\mathbf{f}$ and ${}^B\boldsymbol{\tau}$ are the force and torque needed for the object manipulation defined as

$$\begin{aligned} {}^B\mathbf{f} &= [\,{}^Bf_x \quad {}^Bf_y \quad {}^Bf_z\,]^{\mathrm{T}}, \\ {}^B\boldsymbol{\tau} &= [\,{}^B\tau_x \quad {}^B\tau_y \quad {}^B\tau_z\,]^{\mathrm{T}}. \end{aligned} \tag{7}$$

Note that it is not necessary to set the input vector to be the variable on the right-hand side of (6) when the RNN is trained to learn an inverse dynamics model. For example, the RNN can be trained to acquire an inverse dynamics model as a mapping given by

$$F : x, y, z, \phi, \theta, \psi \rightarrow {}^B\mathbf{f}_N, {}^B\boldsymbol{\tau}_N, \tag{8}$$

where $\phi$, $\theta$, and $\psi$ are the orientation angles (Fig. 4), and the subscript $N$ represents the output of RNN. Concretely, a mapping given by

$$F : \left\{ \begin{matrix} \tilde{x} & \tilde{y} & \tilde{z} & \tilde{\phi} & \tilde{\theta} & \tilde{\psi} \\ \dot{\tilde{x}} & \dot{\tilde{y}} & \dot{\tilde{z}} & \dot{\tilde{\phi}} & \dot{\tilde{\theta}} & \dot{\tilde{\psi}} \\ \ddot{\tilde{x}} & \ddot{\tilde{y}} & \ddot{\tilde{z}} & \ddot{\tilde{\phi}} & \ddot{\tilde{\theta}} & \ddot{\tilde{\psi}} \end{matrix} \right\} \rightarrow {}^B\mathbf{f}_N, {}^B\boldsymbol{\tau}_N \tag{9}$$

is defined as the inverse dynamics model to be acquired here, which generates ${}^B\mathbf{f}$ and ${}^B\boldsymbol{\tau}$ from the six DOF motion of the object. The 18 inputs of the inverse dynamics model are the estimates of the position and orientation and the derivatives calculated by the DOB-type differentiator described in Sec. 2.1. The RNN is applied to the external force estimation. Using ${}^B\mathbf{f}_N$ and ${}^B\boldsymbol{\tau}_N$ calculated from the RNN inverse dynamics model, which is required for manipulation while no external force is applied and the actually measured manipulation force ${}^B\mathbf{f}$ and ${}^B\boldsymbol{\tau}$, the net external force while the object is dynamically manipulated can be calculated as

$$\begin{bmatrix} {}^B\hat{\mathbf{f}}_d \\ {}^B\hat{\tau}_d \end{bmatrix} = \begin{bmatrix} {}^B\mathbf{f}_N \\ {}^B\boldsymbol{\tau}_N \end{bmatrix} - \begin{bmatrix} {}^B\mathbf{f} \\ {}^B\boldsymbol{\tau} \end{bmatrix}. \tag{10}$$

In order to implement the mechanical impedance in the object coordinate system $B$ according to the orientation of the manipulated object, the external force observed from the object coordinate system $B$ is estimated.

### 3.2. *Collision force absorption during object manipulation based on mechanical impedance control*

Collision force absorbing method is realized using the proposed external force estimator, which generates the net external force that includes no manipulation force and mechanical impedance control [27]. Thus, even while the robot manipulates the object with a soft mechanical impedance control, if no external force is applied, little deviation from the reference trajectory will occur. This allows the robot to perform an accurate work keeping the desired mechanical impedance control functioned. In the proposed method, since the force sensor is attached between the end

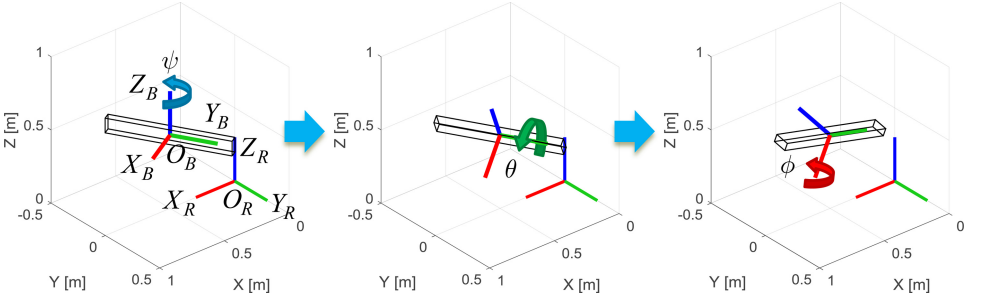


Fig. 4. Definition of orientation of manipulated object, i.e. roll angle $\phi$, pitch angle $\theta$, yaw angle $\psi$ according to the absolute coordinate system $R$.

Un. Sys. 2020.08:239-251. Downloaded from www.worldscientific.com
by CHINESE UNIVERSITY OF HONG KONG on 08/08/20. Re-use and distribution is strictly not permitted, except for Open Access articles.

effector and the object, the external force can be detected no matter where on the object a person touches.

A mechanical impedance control is implemented using the virtual internal model (VIM) [28]. For simplicity, only the case for $X_B$-axis in the object coordinate system $B$ will be explained as an example, and the other axes can be handled in the same way. Let a desired virtual mass, viscosity, and stiffness be $M_t$, $D_t$, and, $K_t$, a VIM in the $X_B$-axis is given by

$$\frac{d}{dt}\begin{bmatrix} {}^{B}x_{\Delta} \\ {}^{B}\dot{x}_{\Delta} \end{bmatrix} = \begin{bmatrix} 0 & 1 \\ -\dfrac{K_t}{M_t} & -\dfrac{D_t}{M_t} \end{bmatrix}\begin{bmatrix} {}^{B}x_{\Delta} \\ {}^{B}\dot{x}_{\Delta} \end{bmatrix} + \begin{bmatrix} 0 \\ \dfrac{1}{M_t} \end{bmatrix} {}^{B}\hat{f}_{dx}. \quad (11)$$

The VIM (11) is discretized at the sampling time of $T_s$ and implemented to generate the trajectory for the compliant motion. Let the reference trajectory for a task in the reference coordinate system $R$ be $[x_r \quad y_r \quad z_r]^{\mathrm{T}}$, by modifying it as

$$\begin{bmatrix} x_d \\ y_d \\ z_d \end{bmatrix} = \begin{bmatrix} x_r \\ y_r \\ z_r \end{bmatrix} + {}^{R}\mathbf{R}_B \begin{bmatrix} {}^{B}x_{\Delta} \\ {}^{B}y_{\Delta} \\ {}^{B}z_{\Delta} \end{bmatrix}, \quad (12)$$

and making the robot follow this reference $[x_d \quad y_d \quad z_d]^{\mathrm{T}}$, a desired mechanical impedance to the net external force in the object coordinate system $B$ is realized, where

$${}^{R}\mathbf{R}_B = \begin{bmatrix} C_\theta C_\psi & S_\phi S_\theta C_\psi - C_\phi S_\psi & C_\phi S_\theta C_\psi + S_\phi S_\psi \\ C_\theta S_\psi & S_\phi S_\theta S_\psi + C_\phi C_\psi & C_\phi S_\theta S_\psi - S_\phi C_\psi \\ -S_\theta & S_\phi C_\theta & C_\phi C_\theta \end{bmatrix}, \quad (13)$$

and $C_\theta = \cos\theta$, $S_\theta = \sin\theta$, $C_\psi = \cos\psi$, and $S_\psi = \sin\psi$.

## 4. Experiment of External Force Estimation

### 4.1. *Collision force absorption during object manipulation based on mechanical impedance control*

Figure 3 in 3.1 shows the experimental setup using a robot, PA10-7C (Mitsubishi Heavy Industries, Ltd.). The object to be manipulated is an aluminum baton, on which a weight movable on the linear guide is installed to apply the external force during the baton manipulation. The weight can be fixed to make no external force generated. Table 1 lists the parameters of the baton and the weight. The equivalent force applied to the COM of the baton is measured by a force sensor (NITTA Corp.) installed between the robot and the baton (Fig. 3). Thus, the force can be detected no matter where on the baton, a person touches. The sampling period of the control including the RNN calculation is 10 ms.

Table 1. Parameter values of aluminum baton and sliding weight supported by a linear guide.

| Definition | Value [Unit] |
|---|---|
| Mass of aluminum baton | 1.80 kg |
| Width/length/height of aluminum baton | 0.03/0.80/0.06 m |
| Mass of sliding weight | 0.14 g |

### 4.2. *Experimental procedure of external force estimation during object manipulation*

First, the baton is manipulated along three kinds of trajectories with the weight fixed, and the RNN inverse dynamics model is trained so as to acquire the force necessary for the baton manipulation with no external force applied. In the experiment, the number of neurons in the hidden layer is six and the number of tap delays is one. Figure 5 shows the averaged trajectories of the COM of the baton manipulated by the robot that tracks the three kinds of trajectories. Hereafter, the three trajectories in the 20-second increments, from the left in Fig. 5, are referred to as Trajectories #1, #2, and #3. Since the start position of the COM of the baton is set to be 0, the offsets of which are 0.38 m in the $X_R$-axis and 0.8 m in the $Z_R$-axis.

Next, the baton is manipulated along Trajectories #1, #2, and #3 with the weight sliding freely. For example, in Trajectory #2, as shown in the sequence photography in Fig. 6, the weight moves from the center of the baton to the negative direction of the $Y_B$-axis and then to the positive direction. Thus, a torque of approximately $\pm 0.26$ N will be generated, since the weight of 0.14 kg is moving $\pm 0.19$ m from the center. In the experiment, it is checked if this torque can be detected while the robot is manipulating the baton.

### 4.3. *Experimental results of inverse dynamics model acquisition by learning*

The input vector to the RNN inverse dynamics model is the 18 states of the baton as described in (9). The derivatives are calculated by the DOB-type differentiator with about 10 Hz bandwidth. The teaching signal is the average of ten sets of the time series of ${}^{B}\mathbf{f}$ and ${}^{B}\boldsymbol{\tau}$ equivalently applied to the COM of the baton during when the baton is being manipulated with no external force. Figure 7 shows the time responses of the output signals ${}^{B}\mathbf{f}_N$ and ${}^{B}\boldsymbol{\tau}_N$ from the trained RNN inverse dynamics model, compared with those of the teaching signals ${}^{B}\mathbf{f}$ and ${}^{B}\boldsymbol{\tau}$. These responses agree well with each other although some influence of noise is observed. The details will be omitted due to the limitation of the page length, the proposed RNN inverse dynamics model was evaluated using unknown

Un. Sys. 2020.08:239-251. Downloaded from www.worldscientific.com
by CHINESE UNIVERSITY OF HONG KONG on 08/08/20. Re-use and distribution is strictly not permitted, except for Open Access articles.

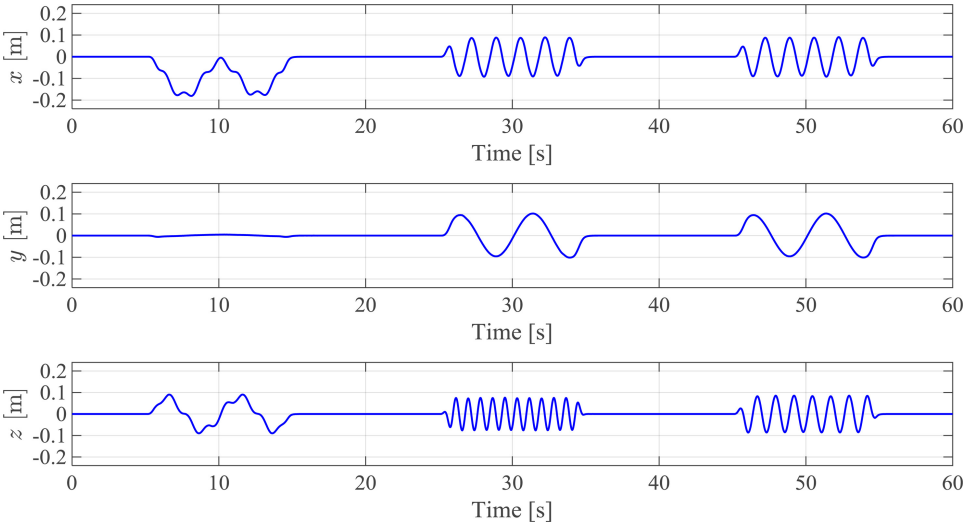


(a) Position of COM of the baton.

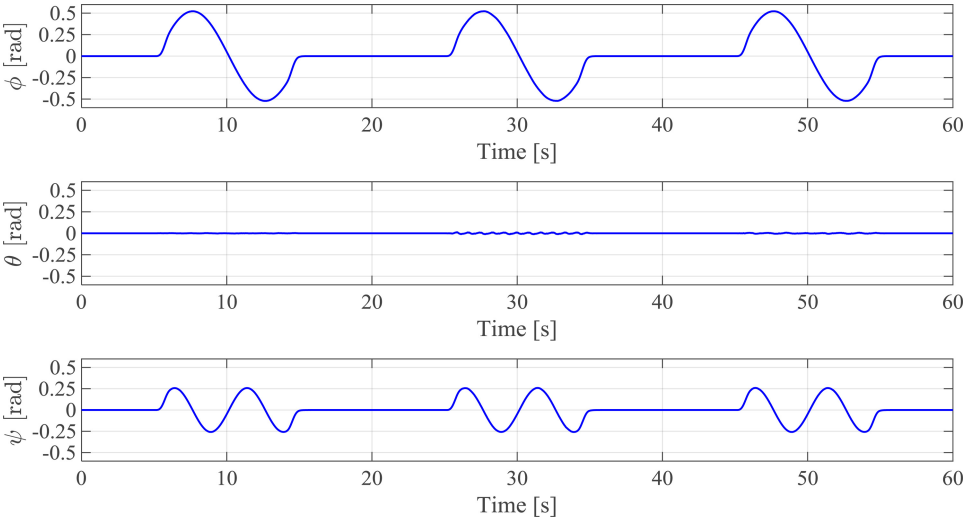


(b) Orientation of the baton: The definition is given in Fig. 4.

Fig. 5. Time responses of the baton trajectories used in training RNN: Three six-DOF trajectories in the 20-second increments from the left are referred to as Trajectories #1, #2, and #3.

trajectories in the six-DOF experiments after trained with random trajectories based on band-limited M sequences, similar to the simulations in [25] by the authors. As a result, it has been confirmed that the RNN inverse dynamics model functions properly even for the unknown trajectories.

### 4.4. *Experimental result of external force estimation*

The external force/torque is calculated by (10). For example, ${}^{B}\hat{\boldsymbol{\tau}}_d$ are calculated as ${}^{B}\boldsymbol{\tau}_N - {}^{B}\boldsymbol{\tau}$ using the measured torque ${}^{B}\boldsymbol{\tau}$ and the RNN output ${}^{B}\boldsymbol{\tau}_N$. The red lines in Fig. 8 show the time responses of the external torque estimate ${}^{B}\hat{\boldsymbol{\tau}}_d$ while the weight is sliding during the baton manipulation as shown in Fig. 6. The graphs in order from the left column correspond to Trajectories #1, #2, and #3, and all the subsequent plots are 4displayed in the same order. As shown in Fig. 8, it has been confirmed that the estimated value of ${}^{B}\hat{\tau}_{dx}$ when the weight is at the end of the linear guide agrees well with the theoretical value of $\pm 0.26\,\mathrm{N}\cdot\mathrm{m}$. For comparison, the time responses of ${}^{B}\hat{\tau}_{dx}$, when no external torque is applied with the weight fixed, are also plotted by blue lines in Fig. 8, and it was about zero during the manipulation.

Un. Sys. 2020.08:239-251. Downloaded from www.worldscientific.com
by CHINESE UNIVERSITY OF HONG KONG on 08/08/20. Re-use and distribution is strictly not permitted, except for Open Access articles.

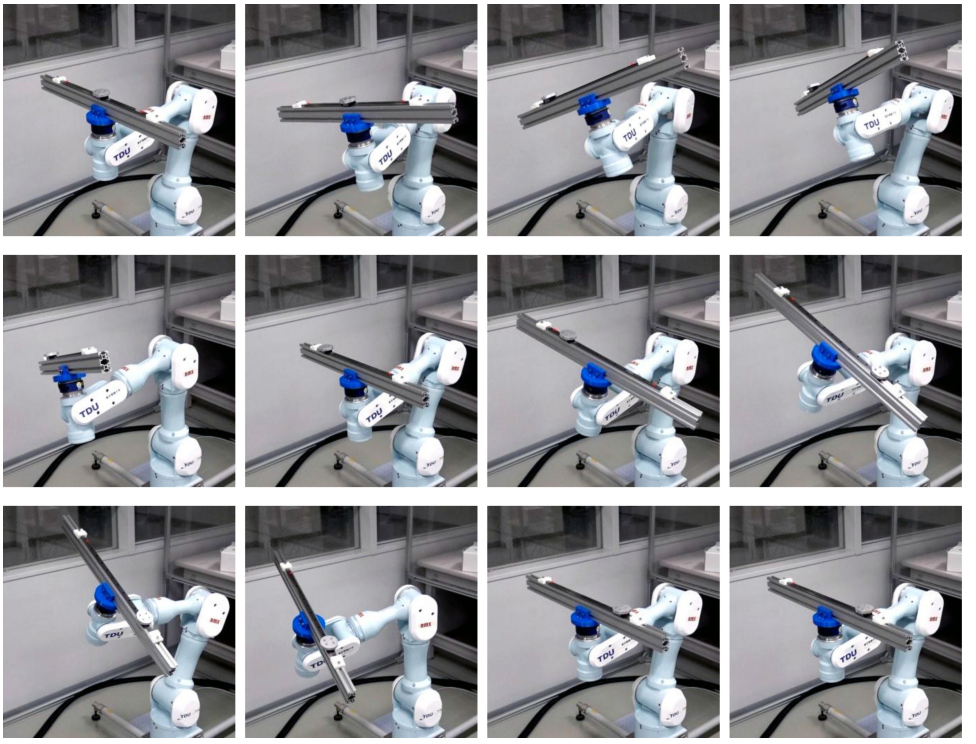

Fig. 6. Sequence photography of Trajectory #2 motion of robot in action as an example, which is captured every second (from left top to right bottom as time progresses): The weight is sliding while the robot is manipulating the baton (see Sec. 4.4 for the detail).

Hereinafter (including Fig. 8), for the sake of making the graphs easy to be recognizable, the time responses are displayed after passing through a low-pass filter with a cutoff of 2 Hz. Note that this filtering is NOT applied when the experiment is in action, and it is only for the display purpose. This is because especially for ${}^{B}\boldsymbol{\tau}$, as shown in Fig. 7(b), high-frequency components are mixed due to the sensor noise and vibration.

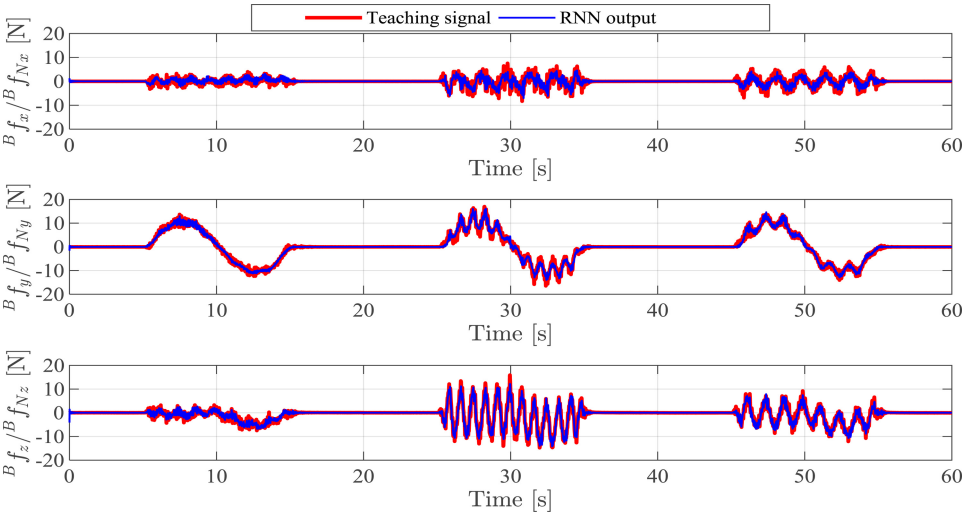


(a) Force observed in the object coordinate system B.

Fig. 7. Time responses of manipulation force/torque ${}^{B}\mathbf{f}$ and ${}^{B}\boldsymbol{\tau}$, i.e. teaching signals and outputs of RNN inverse dynamics model ${}^{B}\mathbf{f}_N$ and ${}^{B}\boldsymbol{\tau}_N$, trained by using Trajectories #1, #2, and #3.

Un. Sys. 2020.08:239-251. Downloaded from www.worldscientific.com
by CHINESE UNIVERSITY OF HONG KONG on 08/08/20. Re-use and distribution is strictly not permitted, except for Open Access articles.

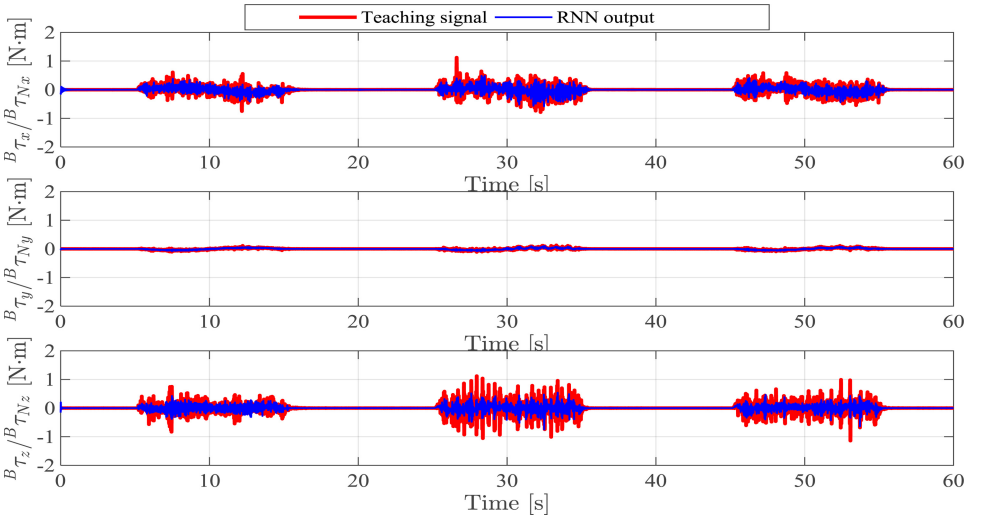


(b) Torque observed in the object coordinate system B.

Fig. 7. (*Continued*)

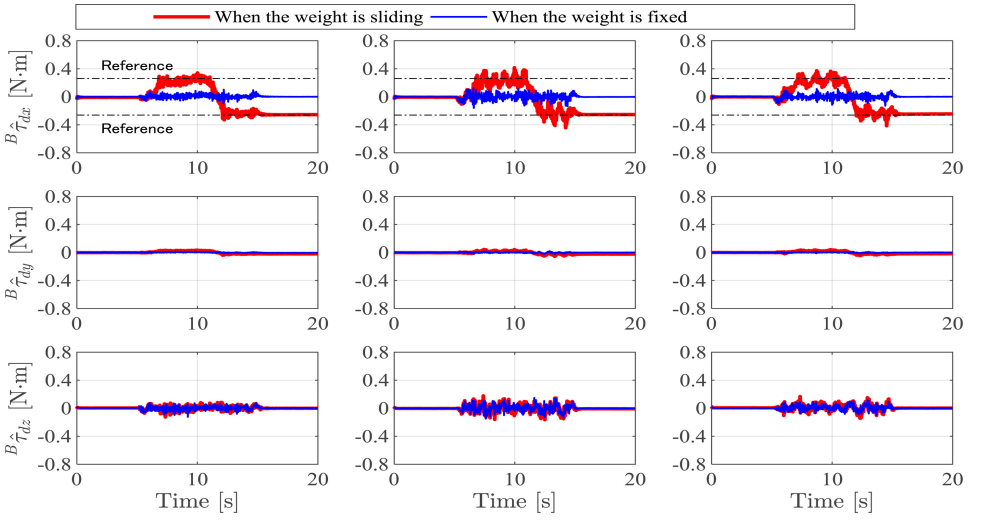


Fig. 8. Time responses of estimated external torque ${}^B\hat{\boldsymbol{\tau}}_d$ calculated by subtracting ${}^B\boldsymbol{\tau}$ from ${}^B\boldsymbol{\tau}_N$, for both the case that the weight is sliding (red line) and fixed (blue line) while the robot is manipulating the baton according to Trajectories #1, #2 and #3: ${}^B\hat{\tau}_{dx}$ around the $X_B$-axis agrees with the theoretical value of $\pm 0.26\,\mathrm{N{\cdot}m}$ $(= \pm 0.19\,\mathrm{m} \times 0.14\,\mathrm{kg} \times 9.81\,\mathrm{m/s^2})$.

## 5. Experiment of Compliant Motion Control During Object Manipulation

### 5.1. *Experimental procedure of applying force to object manipulated by robot*

A mechanical impedance control is implemented so as to react to the net external force estimated by the proposed external force estimator. As a result, the robot can precisely manipulate the object at high speed with the mechanical impedance control functioned to react to the external force. Thus, even if a person accidentally comes in contact with the object, the collision force can be absorbed according to a desired mechanical impedance.

An experiment is conducted in which a person touches (collides) the baton while the robot manipulates it along the Trajectories #1, #2, and #3. The translational impedance parameters $M_t$, $D_t$, and $K_t$ are, respectively, set to be 6.0 kg, 98.0 N/(m/s), and 100.0 N/m in the object coordinate system $B$. The rotational ones $M_t$, $D_t$, and $K_t$ are $1.5\,\mathrm{kg{\cdot}m^2}$, 15.5 N·m/(rad/s), and 10.0 N·m/rad.

Un. Sys. 2020.08:239-251. Downloaded from www.worldscientific.com
by CHINESE UNIVERSITY OF HONG KONG on 08/08/20. Re-use and distribution is strictly not permitted, except for Open Access articles.

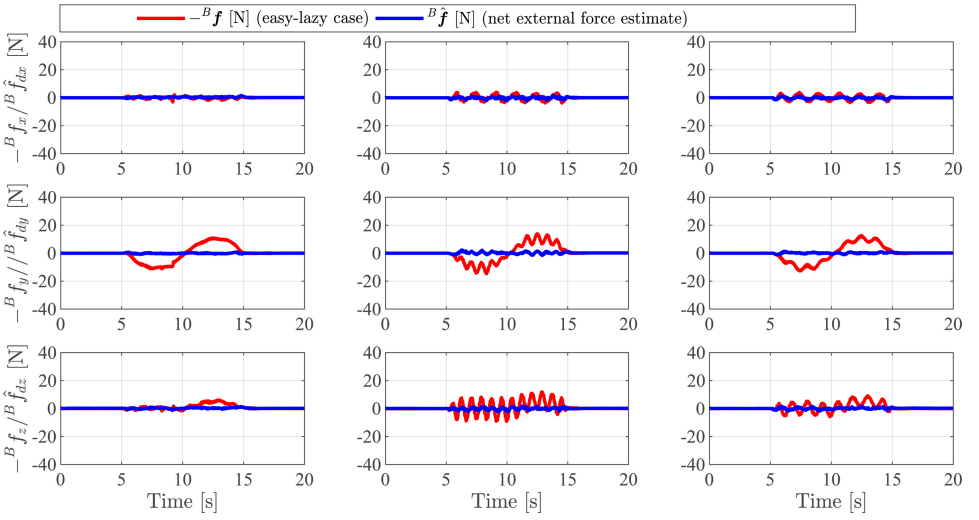


Fig. 9. Comparison of the time responses of a substitute for external force, i.e. $-{}^B\mathbf{f}$ (red line, reverse sign of manipulation force) and net external force estimate ${}^B\hat{\mathbf{f}}_d$ (blue line) calculated by the proposed method while no external force is applied for Trajectory #1, #2, and #3 (from left to right): Note that the force might be used as the substitute only when the manipulated object is in steady state as an easy–lazy implementation.

### 5.2. *Experimental result of mechanical impedance control during baton manipulation with no external force*

Red lines in Fig. 9 show the time responses of $-{}^B\mathbf{f}$ that is an alternative external force in the easy–lazy implementation. Since the value of $-{}^B\mathbf{f}$ reaches a certain amount due to the baton manipulation force even if no external force is applied, the original trajectories of the baton shown by blue lines in Fig. 10 are undesirably modified by the mechanical impedance model driven by $-{}^B\mathbf{f}$. Thus, significant deviations occur as shown in red lines in Fig. 10. On the other hand, as shown by blue lines in Fig. 9, the net external force ${}^B\hat{\mathbf{f}}_d$ is correctly estimated to be almost zero even while the baton is being manipulated with no external force applied. Thus, by driving the mechanical impedance model by ${}^B\hat{\mathbf{f}}_d$, little trajectory deviation occurs (Fig. 11). This means that the proposed method allows the robot to quickly and precisely manipulate the baton with the mechanical impedance control functioned.

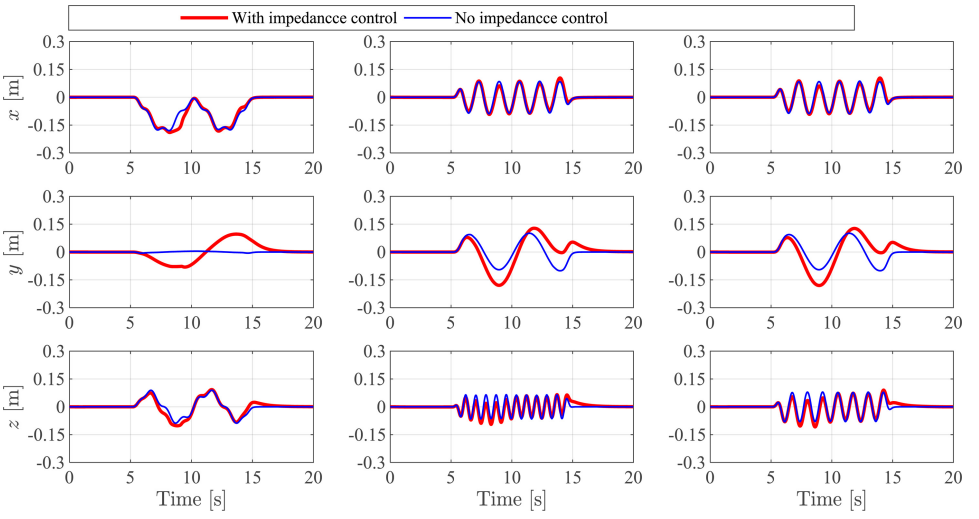


Fig. 10. Time responses of COM trajectories of the baton for Trajectory #1, #2, and #3 with mechanical impedance control driven by $-{}^B\mathbf{f}$ in Fig. 9 (easy–lazy implementation): Compared with the original trajectories (blue line), it is found that significant deviation occurs (red line).

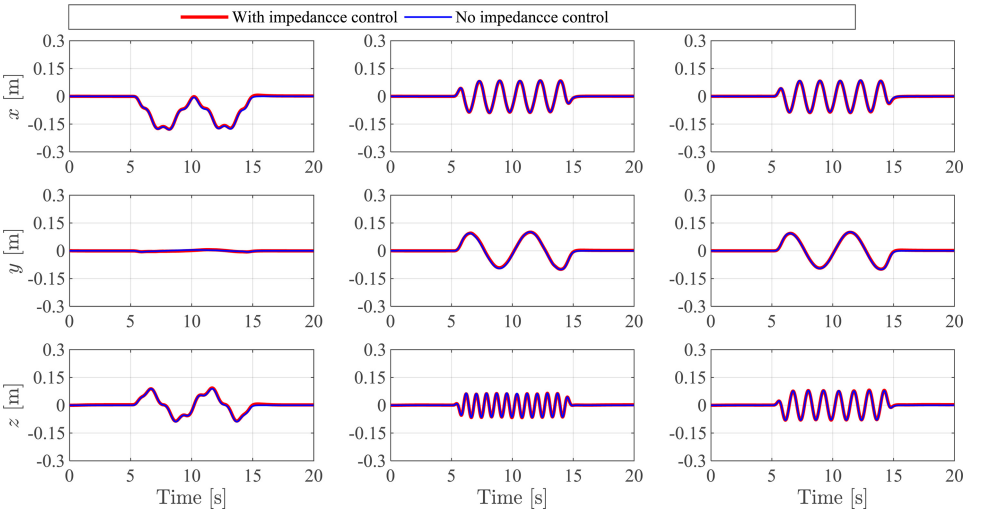


Fig. 11. Time responses of COM trajectories of the baton for Trajectory #1, #2, and #3 with mechanical impedance control driven by ${}^{B}\hat{\mathbf{f}}_d$ in Fig. 9: Compared with the original trajectories (blue line), it is found that little deviation occurs (red line) even while the mechanical impedance control is being functioned.

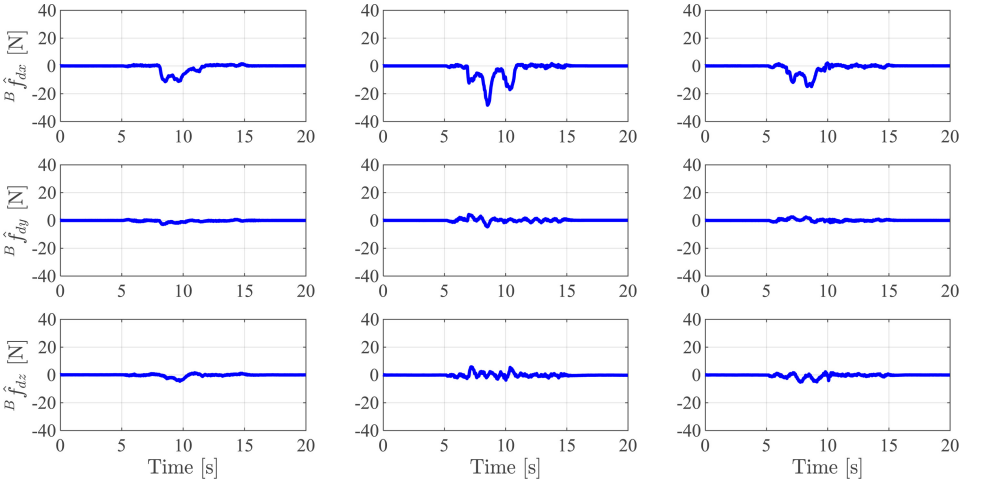


Fig. 12. Time responses of estimated external force ${}^{B}\hat{\mathbf{f}}_d$ in the case that a person applies external force in the $X_B$-direction while the robot is manipulating the baton according to Trajectories #1, #2, and #3.

### 5.3. *Experimental result of collision force absorption*

In the experiment, a person touches the baton manipulated by the robot and applies an external force in the $X_B$-direction. Then, it is checked if the compliant motion to the external force is properly generated. Figure 12 shows the time responses of the external force estimates ${}^{B}\hat{\mathbf{f}}_d$, and Fig. 13 shows the time responses of the baton trajectories and indicates that an appropriate compliant motion is generated. Note that there is no compliant motion generated until the external force is applied and that the baton trajectories start converging to the original trajectories after the application of external force is stopped. Figure 14 shows sequence photography of the compliant motion in the $X_B$-direction for Trajectory #2, compared with the motion without impedance control. From Figs. 13 and 14, it can be seen that the robot gives way to the person and absorbs the collision force according to a desired mechanical impedance model. The same kind of experiment was conducted for the rotational motion, and it has been also confirmed that it works well.

## 6. Conclusion

In this paper, an external force/torque estimator based on an inverse dynamics model using a RNN was proposed. The

Un. Sys. 2020.08:239-251. Downloaded from www.worldscientific.com
by CHINESE UNIVERSITY OF HONG KONG on 08/08/20. Re-use and distribution is strictly not permitted, except for Open Access articles.

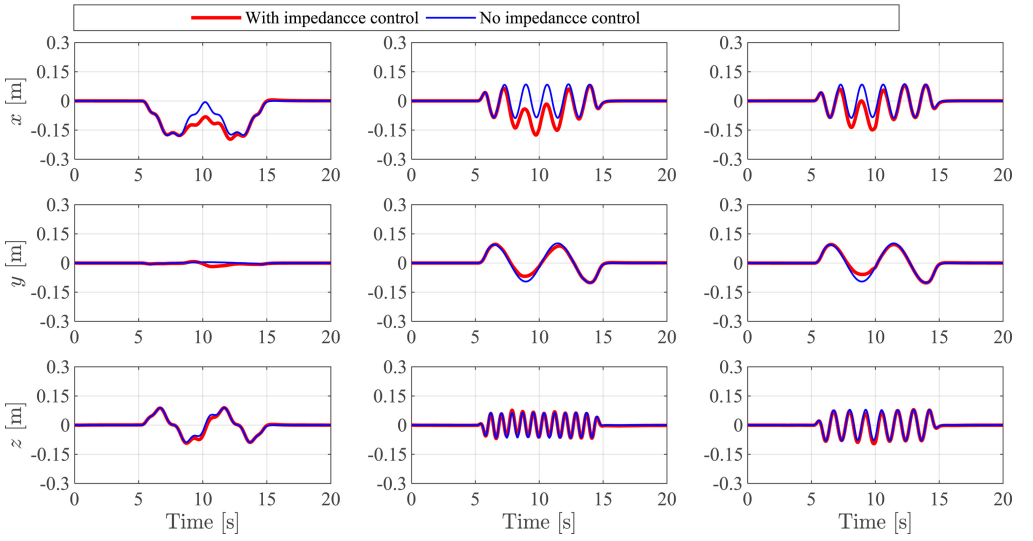


Fig. 13. Time responses of COM trajectories of the baton in the compliant motion to the external force in Fig. 12: Compared with the original trajectories (blue line), it can be seen that the robot gives way to the person (red line) to absorb the contact force even during object manipulation.

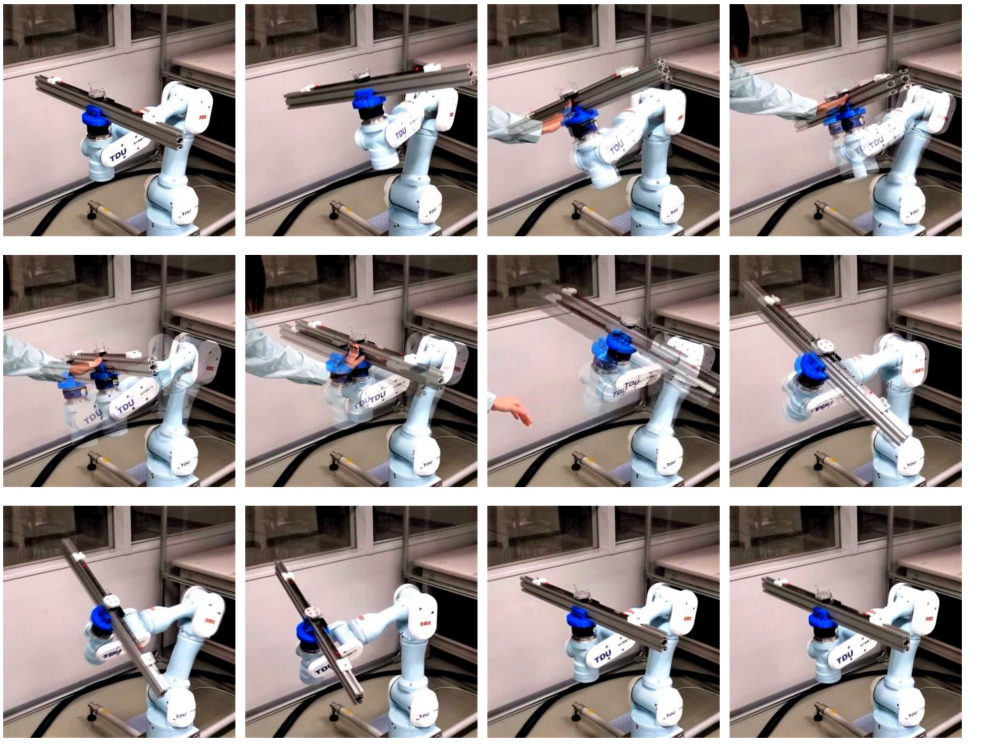

Fig. 14. Sequence photography of compliant motion of robot in the $X_B$-direction for Trajectory #2 corresponding to the duration from 5 s to 16 s in Fig. 13, which is captured every second (from left top to right bottom as time progresses): For comparison, photography of robot in the original trajectory (no impedance control) is composited. Note that the robot flexibly gives way to the person who touches the baton during manipulation.

Un. Sys. 2020.08:239-251. Downloaded from www.worldscientific.com
by CHINESE UNIVERSITY OF HONG KONG on 08/08/20. Re-use and distribution is strictly not permitted, except for Open Access articles.

Un. Sys. 2020.08:239-251. Downloaded from www.worldscientific.com
by CHINESE UNIVERSITY OF HONG KONG on 08/08/20. Re-use and distribution is strictly not permitted, except for Open Access articles.

estimator has been successfully worked to estimate the net external force/torque, distinguishing it from the object manipulation force/torque of the robot. The effectiveness has been confirmed by experiment where the external torque is applied while the robot is dynamically manipulating an object and is estimated by the proposed method.

By using the proposed estimator combined with a mechanical impedance control, even while the robot manipulates the object, the robot can seamlessly transit from the accurate manipulation to the compliant motion according to the net external force. The validity of the proposed method has been confirmed by experiments in which a person touches a manipulated object while the robot was dynamically handling the object.

## References

[1] B. Chen, J. Wan, L. Shu, P. Li, M. Mukherjee and B. Yin, Smart factory of industry 4.0 key technologies, application case, and challenges, *IEEE Access* **6** (2018) 6505–6519.

[2] Japanese Ministry of Economy, Trade and Industry (METI), Explore collaborations of the next generation: the scene where humans and robots are cooperating, *METI J.* (2014) (in Japanese), http://www.meti.go.jp/publication/data/newmeti_j/141011.pdf.

[3] C. Vogel, M. Fritzsche and N. Elkmann, Safe human-robot cooperation with high-payload robots in industrial applications, in *Proc. 2016 11th ACM/IEEE Int. Conf. Human-Robot Interaction (HRI)* (Christchurch, New Zealand, 2016), pp. 529–530.

[4] S. Lee, Y. Kim and J. Song, Novel collision detection index based on joint torque sensors for a redundant manipulator, in *Proc. 2013 IEEE/RSJ Int. Conf. Intelligent Robots and Systems*, Vol. 1 (Tokyo, Japan, 2013), pp. 4636–4641.

[5] S. Lee, M. Kim and J. Song, Sensorless collision detection for safe human-robot collaboration, in *Proc. 2015 IEEE/RSJ Int. Conf. Intelligent Robots and Systems* (Hamburg, Germany, 2015), pp. 2392–2397.

[6] B. Jung, H. R. Choi, J. C. Koo and H. Moon, Collision detection using band designed disturbance observer, in *Proc. 2012 IEEE Int. Conf. Automation Science and Engineering (CASE)* (Seoul, Korea, 2012), pp. 1080–1085.

[7] J. Park, Y. Lee, J. Song and H. Kim, Safe joint mechanism based on nonlinear stiffness for safe human-robot collision, in *Proc. 2008 IEEE Int. Conf. Robotics and Automation* (Pasadena, California, USA, 2008), pp. 2177–2182.

[8] Y. Kim, Anthropomorphic low-inertia high-stiffness manipulator for high-speed safe interaction, *Proc. IEEE Trans. Robot.* **33** (2017) 1358–1374.

[9] Y. Sugahara *et al.*, Experimental study on manipulator design for low collision impact force, in *Proc. 2009 IEEE/ASME Int. Conf. Advanced Intelligent Mechatronics* (Singapore, 2009), pp. 899–904.

[10] H. Lim, K. Maenisi and M. Sunagawa, Development of collision force suppression mechanism, in *Proc. 2008 IEEE Int. Conf. Control, Automation and Systems* (Seoul, Korea, 2008), pp. 2032–2037.

[11] R. M. Ahmed and I. Kalaykov, Static and dynamic collision safety for human robot interaction using magneto-rheological fluid based compliant robot manipulator, in *Proc. 2010 IEEE Int. Conf. Robotics and Biomimetics* (Tianjin, China, 2010), pp. 370–375.

[12] M. Kawazawa, S. Sakaino and T. Tsuji, High backdrivability control based on estimation of shaft torsion using load side angle sensor, *IECON 2018 — 44th Annual Conf. IEEE Industrial Electronics Society* (Washington D.C., USA, 2018), pp. 5457–5462.

[13] A. Hasegawa, H. Fujimoto and T. Takahashi, Filtered disturbance observer for high backdrivable robot joint, in *IECON 2018 — 44th Annual Conf. IEEE Industrial Electronics Society* (Washington D.C., USA, 2018), pp. 5086–5091.

[14] X. Sun *et al.*, Design and control of a novel robotic knee-ankle prosthesis system, in *Proc. 7th IEEE Int. Conf. Biomedical Robotics and Biomechatronics* (Twente, Netherlands, 2018), pp. 737–743.

[15] A. Ortlieb *et al.*, An active impedance controller to assist gait in people with neuromuscular diseases: Implementation to the hip joint of the AUTONOMYO exoskeleton, in *Proc. 7th IEEE Int. Conf. Biomedical Robotics and Biomechatronics* (Twente, Netherlands, 2018), pp. 537–543.

[16] C. B. Sanz-Morere *et al.*, A bioinspired control strategy for the CYBERLEGs knee-ankle-foot orthosis: Feasibility study with lower-limb amputees, in *Proc. 7th IEEE Int. Conf. Biomedical Robotics and Biomechatronics* (Twente, Netherlands, 2018), pp. 503–508.

[17] S. Crea *et al.*, A novel shoulder-elbow exoskeleton with series elastic actuators, in *Proc. 2016 6th IEEE Int. Conf. Biomedical Robotics and Biomechatronics* (University Town, Singapore, 2016), pp. 1248–1253.

[18] T. Lens and O. von Stryk, Investigation of safety in human-robot-interaction for a series elastic, tendon-driven robot arm, in *Proc. 2012 IEEE/RSJ Int. Conf. Intelligent Robots and Systems* (Vilamoura, Algarve, Portugal, 2012), pp. 4309–4314.

[19] J. Ishikawa, A. Sakai and K. Furuta, Object dynamics virtualization by robotic assistance for cooperative object handling with human, in *Proc. 2009 IEEE/RSJ Int. Conf. Intelligent Robots and Systems* (St. Louis, USA, 2009), pp. 4238–4244.

[20] M. Nakao, K. Ohnishi and K. Miyachi, A robust decentralize joint control based on interference estimation, in *Proc. IEEE Int. Conf. Robotics and Automation* (Raleigh, North Carolina, USA, 1987), pp. 326–331.

[21] S. Yamada and J. Ishikawa, Nonlinear disturbance observer with recurrent neural network compensator, in *Proc. 5th Int. Conf. Advanced Engineering — Theory and Applications (AETA)* (Ho Chi Minh, Vietnam, 2017).

[22] J. Li *et al.*, Design of neural network disturbance observer using RBFN for complex nonlinear systems, in *Proc. 30th Chinese Control Conf.* (Yantai, China, 2011), pp. 6187–6192.

[23] J. Ma *et al.*, Neural network disturbance observer based controller of an electrically driven stewart platform using backstepping for active vibration isolation, in *Proc. Int. Joint Conf. Neural Networks* (Atlanta, Georgia, USA, 2009), pp. 1939–1944.

[24] N. Ishibashi and Y. Maeda, Learning of inverse-dynamics for SCARA robot, *SICE Annual Conf.* (Tokyo, Japan, 2011), pp. 1300–1303.

[25] M. Hanafusa and J. Ishikawa, External force estimation for nonlinear systems using recurrent neural network, in *Proc. IEEE/ASME Int. Conf. Advanced Intelligent Mechatronics (AIM 2019)* (Hong Kong, China, 2019), pp. 1055–1061.

[26] M. H. Beale, M. T. Hagan and H. B. Demuth, *MATLAB Neural Network Toolbox Getting Started Guide* (MathWorks Inc., 2016).

[27] N. Hogan, Impedance control: An approach to manipulation, part I, II, III, *ASME J. Dyn. Syst. Meas. Control* **101** (1985) 1–24.

[28] K. Kosuge, K. Furuta and T. Yokoyama, Virtual internal model following control of robot arms, in *Proc. 1987 IEEE Int. Conf. Robotics and Automation*, Vol. 4 (Raleigh, North Carolina, USA, 1987), pp. 1549–1554.

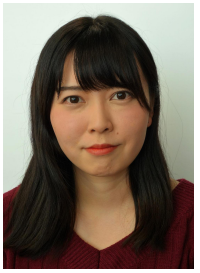

**Misaki Hanafusa** received her Bachelor of Engineering from Tokyo Denki University, Japan, in 2019. She is currently a Graduate Student of Tokyo Denki University, Japan.

Her research interests include human cooperative robotics, human-machine interaction, and soft robotics.

Misaki Hanafusa is a Member of the Robotic Society of Japan.

**Jun Ishikawa** received his B.E. and M.E. degrees in Control Engineering from the Tokyo Institute of Technology in 1989 and 1991, respectively. He joined NEC Corporation in 1991, as a Research Engineer of Mechatronics and Computer Peripherals and had also been a Visiting Industrial Fellow at the University of California, Berkeley from 1996 to 1997. He received his Doctor of Engineering degree from the Tokyo Institute of Technology in 1999. He was a Research Manager of the R&D Office for Supporting Antipersonnel Mine Detection and Removal Activities, Japan Science and Technology Agency from 2002 to 2007 and has been a Professor of the Department of Robotics and Mechatronics, Tokyo Denki University since 2007.

His research interests include control theory and its applications to various mechanical systems, e.g. soft robotics, motion control of robots for improving human quality of life, nanoscale servo systems, and equipment for humanitarian demining.

Jun Ishikawa is a Member of the Society of Instrument and Control Engineers, the Japan Society of Mechanical Engineers, the Robotic Society of Japan, the Institute of Electrical and Electronics Engineers.

Un. Sys. 2020.08:239-251. Downloaded from www.worldscientific.com
by CHINESE UNIVERSITY OF HONG KONG on 08/08/20. Re-use and distribution is strictly not permitted, except for Open Access articles.